IEEE Access
Multidisciplinary | Rapid Review | Open Access Journal

Received February 25, 2019, accepted March 6, 2019, date of publication March 18, 2019, date of current version April 3, 2019.

Digital Object Identifier 10.1109/ACCESS.2019.2905683

Reconfigurable Wideband Filtering Balun With Tunable Dual-Notched Bands Using CPW-to-Slot Transition and Varactor-Loaded Shorted-Slot

JIE ZHOU, (Student Member, IEEE), HUIZHEN JENNY QIAN, JIYUAN REN, AND XUN LUO, (Senior Member, IEEE)

Center for Integrated Circuits, University of Electronic Science and Technology of China, Chengdu 611731, China

Corresponding authors: Huizhen Jenny Qian (huizhenqian@hotmail.com) and Xun Luo (xun-luo@ieee.org)

This work was supported in part by the National Natural Science Foundation of China under Grant 61601089.

ABSTRACT In this paper, a reconfigurable wideband filtering balun with tunable dual-notched bands is proposed, using coplanar waveguide (CPW)-to-slot transitions and varactor-loaded shorted-slots. The wideband filtering balun consists of a triple-mode slot resonator, two CPW-to-slot transitions, and a CPW short-stub. Three transmission poles are allocated by the triple-mode slot resonator to achieve the wideband operation. To further improve the amplitude- and phase-imbalance responses, two CPW-to-slot transitions are used. Besides, the CPW short-stub is introduced to enhance the passband selectivity. Then, based on the proposed wideband filtering balun, a reconfigurable balun with tunable dual-notched bands is achieved by introducing two pairs of varactor-loaded shorted-slots. The measured results show that the frequency tuning ranges of the dual-notched bands are 1.28–1.58 GHz (21.6%) and 1.89–2.41 GHz (24.2%) with 15-dB rejection, respectively. The proposed filtering balun shows the advantages of wide fractional bandwidth, high selectivity, low insertion loss, and tunable notched band operation.

INDEX TERMS Balun, coplanar waveguide (CPW), notch, reconfigurable, slot, wideband.

I. INTRODUCTION

The ever increasing demand for compact modern microwave wireless communication systems leads to the requirement of highly integrated multi-function microwave circuits, especially the passive components. Therefore, a significant number of researches have been conducted to realize the integration of baluns and filters. Then, many filtering baluns have been reported [1]–[12]. By using some special technologies, such as low temperature co-fired ceramic (LTCC) technology [1], multilayer organic Liquid Crystal Polymer (LCP) substrate [2], and patterned Permalloy thin film [3], filtering baluns with minimized size have been proposed. However, the structures and design procedures are very complicated because of the complex processing technologies. Based on the Printed Circuit Board (PCB) processing, a compact microstrip filtering balun using the hybrid resonator [4] exhibits a easy design procedure with good in-band performance but poor stopband response. To improve the stopband response, several filtering baluns have been developed based on the conversion from balanced filters [5]–[8]. Nevertheless, the narrow bandwidth performance limits their applications in the practical wideband systems. To further extend the bandwidth of filtering baluns, the high-order planar structure [9], multimode stepped-impedance resonator [10], asymmetric coupled-section [11], and broadside-coupled microstrip/slotline resonator structure [12] are proposed. Nevertheless, the in-band performances still need to be improved.

Recently, microstrip-to-slot transitions have been reported to implement the wideband passive circuits, such as filter [13], power divider [14], and filtering baluns [15]–[17]. A compact out-of-phase uniplanar microstrip power divider (balun) operating over an ultra-wide frequency band is presented [15], which can offer good in-band performance. Then, to further improve the selectivity of filtering baluns, balun based on the triple-mode slotline with microstrip-to-slot transitions is implemented in [16]. However, the microstrip impedances and guided-wavelength characteristics are very sensitive to the substrate thickness. Then, coplanar waveguide (CPW) is introduced to form the transitions [17], which allows a wide range of impedance

The associate editor coordinating the review of this manuscript and approving it for publication was Jaime Laviada.

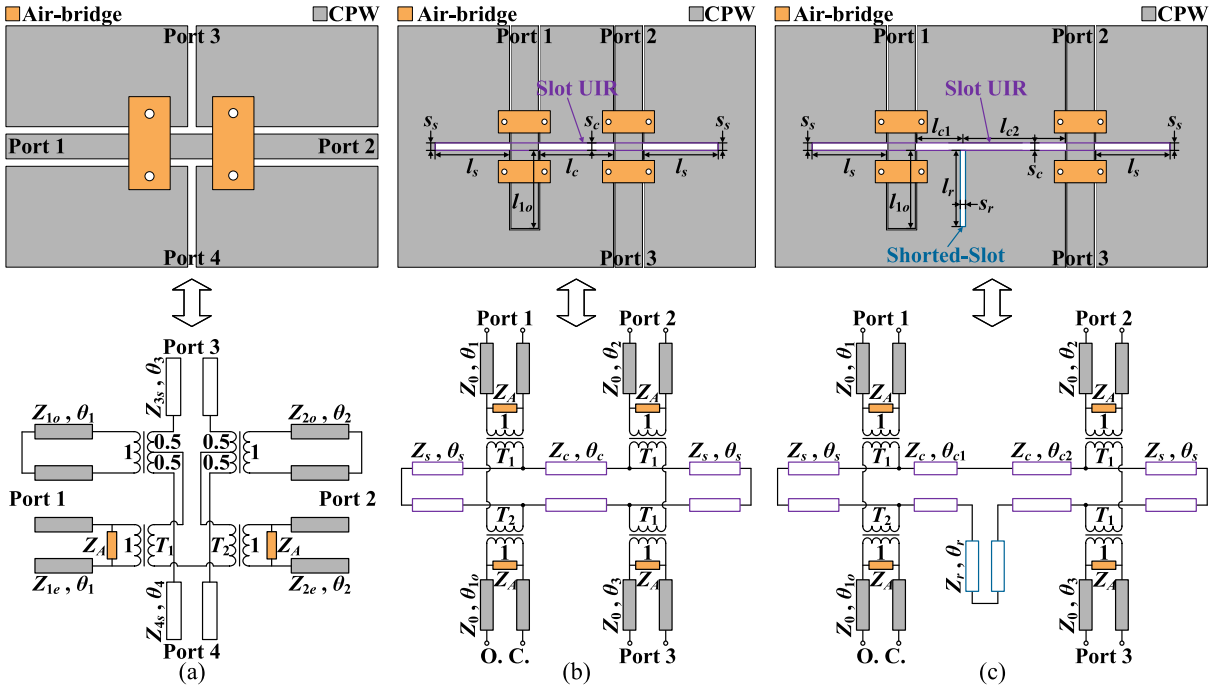

FIGURE 1. (a) The layout and simplified equivalent transmission-line model of the CPW-to-slot transition with air-bridges. Balun prototypes (b) without and (c) with the shorted-slot.

values on relatively thick substrates. Besides, the circuit model of the CPW cross-junction is simple, intuitive, and general. This transition has been used to construct a wideband CPW balun that is uniplanar and does not require any vias [17]. Nevertheless, the existing wireless network signals may interfere the wideband signal propagation for the modern application. To suppress the existed signal interferences in the operation band, notch filters based on the terminated cross-shaped resonators [18] and varactor-loaded microstrip stubs [19] are introduced. However, there is still not a research on wideband filtering balun with notches for interference suppression. Therefore, the design of a wideband filtering balun with good selectivity, excellent in-band balance, and fixed/tunable notched band operation is still a great challenge.

The preliminary work of this paper is published in our conference paper [20] as a wideband filtering balun. Compared to the previous work, a deep analysis on balun prototype using the proposed CPW-to-slot transition with air-bridges and baluns with merits of wideband, low insertion loss, high selectivity, and fixed/tunable notched band operation are proposed in this paper. Firstly, the CPW-to-slot transition is introduced with the related analysis of CPW cross-junction equivalent circuit model to implement the balun prototypes. Meanwhile, to suppress the parasitic odd mode and ensure single TEM mode operation, air-bridges between the ground planes are applied. Secondly, based on the balun prototype using the proposed transitions, a wideband filtering balun operated from 1.03 GHz to 3.17 GHz is implemented. Finally, shorted-slots without and with loaded varactors are used to achieve fixed and tunable notched bands, respectively. The tuning range of the tunable dual-notched bands are 1.28–1.58 GHz (21.6%) and 1.89–2.41 GHz (24.2%) with a 15-dB rejection, respectively. The paper is organized as follows. Section II-A shows the schematic and operation of the balun prototypes using the proposed CPW-to-slot transition. Then, filtering balun with fixed frequency notch and reconfigurable balun with tunable dual-notched bands based on the proposed balun prototype are depicted in Section II-B and C, respectively. The measurement results of these baluns are presented in Section III. Finally, a conclusion is given in Section IV.

II. SCHEMATIC AND OPERATION

A. BALUN PROTOTYPE

Fig. 1(a) shows the layout and simplified equivalent transmission-line model of the CPW-to-slot transition. The proposed transmission-line model is based on the previously published model in [14], which provides insights to the circuit operation. The proposed transition has four port terminations. Port 1 and Port 2 are the CPW, while Port 3 and Port 4 are the slot. Besides, the air-bridges with an equivalent reactance Z_A are placed above the CPW-to-slot transition to suppress the parasitic odd mode. Then, combined the CPW-to-slot transition with a slot uniform impedance resonator (UIR), a balun prototype is achieved, as shown in Fig. 1(b). Frequency responses with uniform magnitude and 180° phase difference are introduced by the slot UIR with CPW-to-slot transitions. The slot is introduced as a multi-mode resonator and the feed lines are CPWs at the two sides. As discussed in [21], the CPW-to-slot coupling strength achieves its maximal

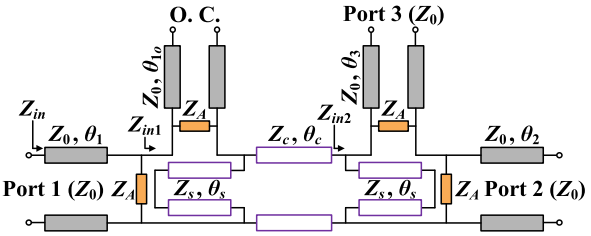

FIGURE 2. Simplified circuit model of the balun prototype in Fig. 1(b).

value, assuming that the length of the open-circuited stub (i.e., l_{1o}) is equal to one quarter guided-wavelength. In addition, the emergence of two transmission poles is due to two resonant modes in the slot resonator. At the junction of the CPW-to-slot transition, the 1:1 transformer is detached (i.e., $T_1 = T_2 = 1$). Then, the simplified equivalent circuit model of the balun prototype illustrated in Fig. 1(b) is shown in Fig. 2. As for a lossless balun network, the theoretical S-parameters could be obtained as

$$S_{11} = \left|\frac{Z_{in} - Z_0}{Z_{in} + Z_0}\right| \tag{1}$$

$$S_{21} = -S_{31} = \frac{1}{\sqrt{2}}\sqrt{1 - \left|\frac{Z_{in} - Z_0}{Z_{in} + Z_0}\right|^2}. \tag{2}$$

It is obvious that the return loss (i.e., S_{11}) and insertion loss (i.e., $S_{2,31}$) are only determined by the input impedance looking from Port 1 (i.e., Z_{in}), which is calculated as

$$Z_{in} = Z_0 \frac{Z_A Z_{in1} + jZ_0(Z_A + Z_{in1})\tan\theta_1}{Z_0(Z_A + Z_{in1}) + jZ_A Z_{in1}\tan\theta_1} \tag{3}$$

$$Z_A = R_s + j\omega L_s + \frac{1}{j\omega C_s} \tag{4}$$

$$Z_{in2} = \frac{j2Z_A Z_0 Z_s \tan\theta_s}{2Z_A Z_0 + j(Z_A + Z_0)Z_s \tan\theta_s} \tag{6}$$

where the impedances (i.e., Z_s and Z_c) and electrical lengths (i.e., θ_s and θ_c) could be obtained from the physical width (i.e., s_s and s_c) and length (i.e., l_s and l_c) of the slot UIR [22], respectively. The detailed calculated procedure is shown in Appendix-A.

Air-bridge is utilized to suppress the unwanted modes, such as the slot mode. As discussed in [23], the enhanced air-bridge structure behaves like a series resonator, and it can approximately be modeled as a series RLC resonator. The layout and simplified model are shown in Fig. 3(a) and (b), respectively. In order to get the approximate parameters for the simplified series resonator model, the equations given in [24] are used to calculate, as discussed in Appendix-B. The extracted element values of the simplified model are

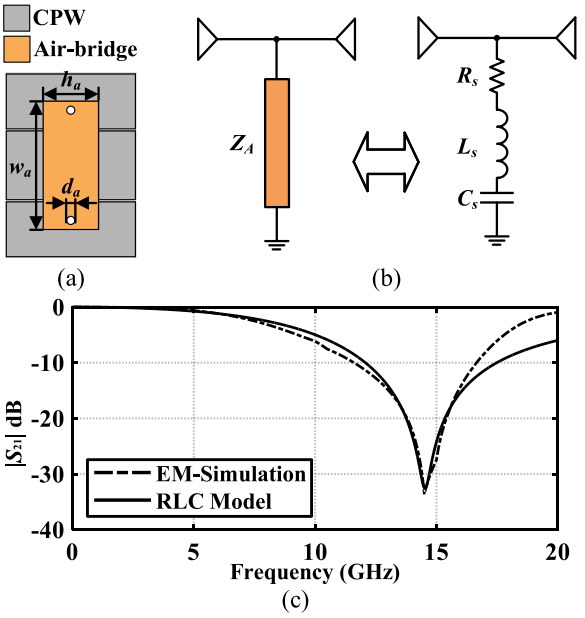

FIGURE 3. (a) Top view of the air-bridge based on RT5880 with $\epsilon_r = 2.2$ and $h = 0.508$ mm ($w_a = 7$ mm, $h_a = 3$ mm, and $d_a = 0.4$ mm). (b) Simplified RLC resonator of the proposed air-bridge. (c) Comparison between EM-simulation and simplified RLC model simulation.

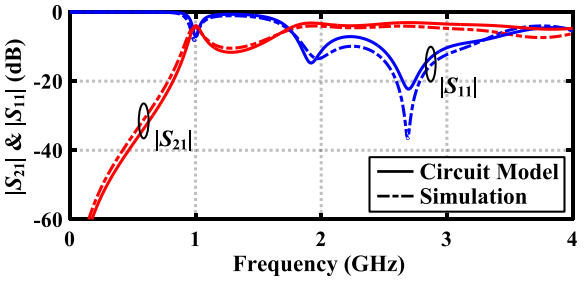

FIGURE 4. Comparison between circuit model and simulation of the balun prototype in Fig. 1(b) ($l_c = 100$ mm, $l_s = 10$ mm, $l_{1o} = 9$ mm, and $s_c = s_s = 1.5$ mm).

$R_s = 0.6\ \Omega$, $L_s = 0.25$ nH, and $C_s = 0.48$ pF under the case of $w_a = 7$ mm, $h_a = 3$ mm, and $d_a = 0.4$ mm, respectively. Fig. 3(c) shows the comparison between EM-simulation of the air-bridge and simplified RLC models, which shows a good agreement between each other. Then, the theoretical S-parameters of the lossless three-port balun network can be calculated. To verify the mechanisms, the balun prototype shown in Fig. 1(b) is implemented on a RT5880 substrate with thickness h of 0.508 mm and dielectric constant ϵ_r of 2.2. Fig. 4 shows the comparison between the circuit model and simulation results, which shows a good agreement. Note that, the end-effect in shorted-slot is considered in the calculation of circuit model [25].

$$Z_{in1} = -\frac{jZ_A Z_0 \cot\theta_{1o}}{Z_A - jZ_0 \cot\theta_{1o}} + \frac{jZ_c Z_s (Z_{in2} + jZ_c \tan\theta_c)\tan\theta_s}{Z_c(Z_{in2} + jZ_c \tan\theta_c) + jZ_c Z_s \tan\theta_s - Z_{in2} Z_s \tan\theta_s \tan\theta_c} \tag{5}$$

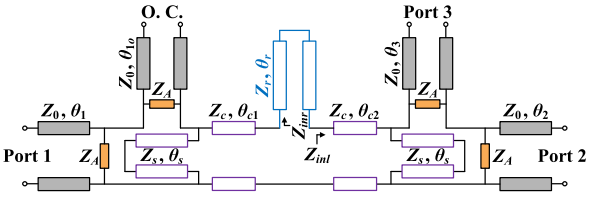

FIGURE 5. Simplified circuit model of the balun prototype with the shorted-slot in Fig. 1(c).

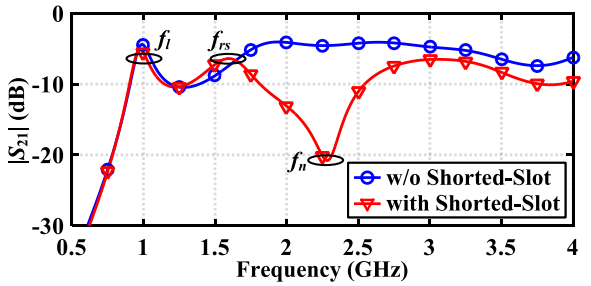

FIGURE 6. EM-simulation frequency responses of the balun prototype with and without the shorted-slot. (l_c = 100 mm, l_{c1} = 30 mm, l_{c2} = 70 mm, l_s = 10 mm, l_{1o} = 9 mm, l_r = 30 mm, s_c = s_s = 1.5 mm, and s_r = 0.5 mm).

For the suppression of interferences in the operation band, the shorted-slot is introduced taped at the slot UIR, as shown in Fig. 1(c). The corresponding simplified circuit model of the notched balun prototype illustrated in Fig. 1(c) is shown in Fig. 5. When input impedance (i.e., Z_{inr}) of the shorted-slot is infinite, the signal power would not be able to be transmitted to the next stage, which leads to a transmission zero f_n (i.e., notch) in the passband, as shown in Fig. 6. Meanwhile, Z_{inr} could be obtained as

$$Z_{inr} = jZ_r \tan\theta_r \tag{7}$$

where Z_r is the characteristic impedance of the shorted-slot. Therefore, the electrical length (i.e., θ_r) of the shorted-slot at the notch frequencies is satisfied with

$$\theta_r = (2n+1)\frac{\pi}{2}, \quad (n = 0, 1, 2, \ldots). \tag{8}$$

As shown in Fig. 6, the proposed shorted-slot can not only introduce a transmission zero (i.e., f_n) but also a resonance (i.e., f_{rs}), simultaneously. The resonant frequency (i.e., f_{rs}) of the shorted-slot is depended on the electrical length θ_{rs} (i.e., $\theta_r + \theta_{c1} + \theta_s$), just like the resonant frequency (i.e., f_l) of the UIR is determined by θ_u (i.e., $2\theta_s + \theta_c$, where $\theta_c = \theta_{c1} + \theta_{c2}$) [16]. Therefore, this resonant frequency f_{rs} can be controlled and adjusted relying on θ_r. Fig. 7 depicts the normalized resonant frequencies of the shorted-slot, i.e., f_{rs}/f_l versus t, where $t = \theta_r/\theta_u$. As shown in Fig. 7, with t increasing, the normalized resonant frequency would decrease. The normalized frequency of the narrow notched band (i.e., f_n/f_l) with respect to electrical length ratio (i.e., t) is also simulated as plotted in Fig. 7. Note that, over the range of t, f_{rs}/f_l is still smaller than f_n/f_l. Therefore, the notched band frequency

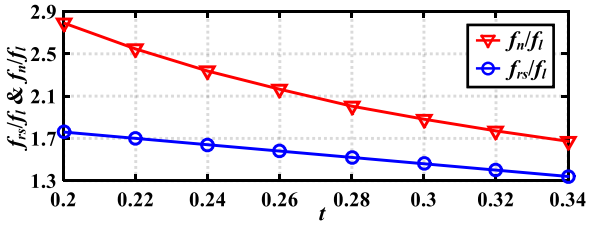

FIGURE 7. Normalized resonant frequency (f_{rs}/f_l) and transmission zero frequency (f_n/f_l) versus electrical length ratio of proposed shorted-slot ($t = \theta_r/\theta_u$).

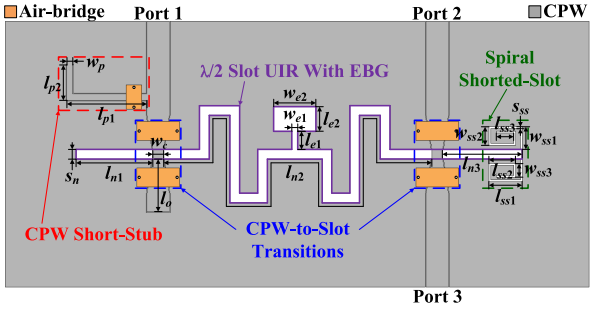

FIGURE 8. Configuration of the proposed wideband filtering balun.

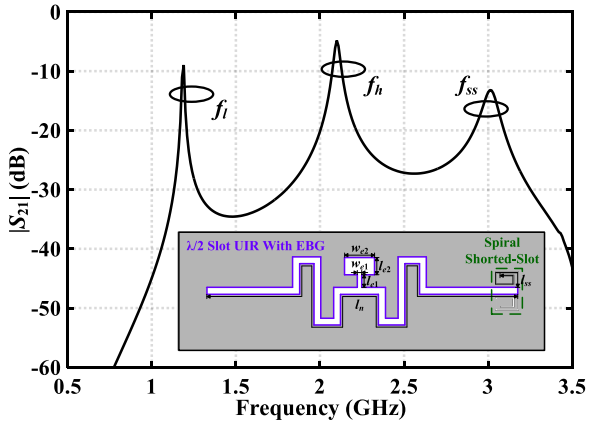

FIGURE 9. EM-simulated frequency response of the proposed λ/2 slot UIR with EBG and spiral shorted-slots.

(i.e., f_n) can be appropriately allocated higher than the resonant frequency (i.e., f_{rs}).

To further enhance the passband performance of the balun prototype in Fig. (b), the CPW short-stub, electromagnetic bandgap (EBG) structure, and a pair of shorted-slots are introduced, as shown in Fig. 8. The wideband operation is mainly achieved by the triple-mode slot resonator, which consists of the slot UIR with EBG and shorted-slots. As shown in Fig. 9, the triple-mode slot resonator could provide three split resonances (i.e., f_l, f_h, and f_{ss}) in the passband. Here, the triple-mode slot resonator is meandered to minimize the size of the proposed balun, which would lead to a slight effect on the split resonances. Meanwhile, a transmission zero f_{zs} upper the passband could also be generated by the pair of

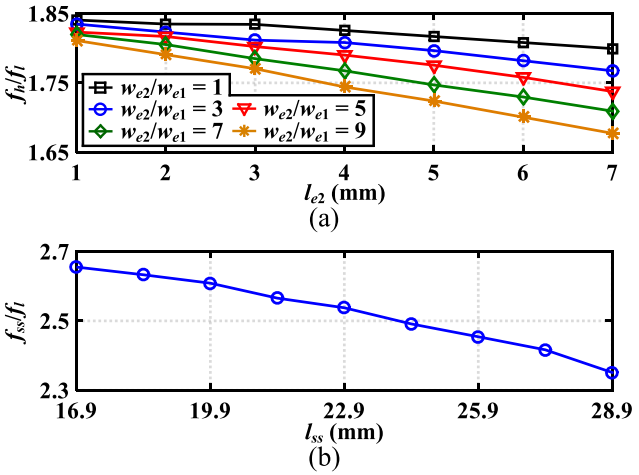

FIGURE 10. (a) Normalized resonant frequency (f_h/f_l) of the proposed triple-mode slot versus the length l_{e2} with different width ratios (l_{e1} = 3 mm and w_{e1} = 1 mm). (b) Normalized resonant frequency (f_{ss}/f_l) of the proposed triple-mode slot versus the length l_{ss} (s_{ss} = 0.3 mm).

the shorted-slot [26], [27]. The split resonances f_l and f_{ss} are determined by the length l_n and l_{ss} of the slot UIR and shorted-slot, respectively. Meanwhile, f_h is about twice of f_l and could be adjusted by tuning the practical dimensions of the EBG structure [20]. The normalized frequencies f_h/f_l and f_{ss}/f_l of the proposed triple-mode slot resonator versus the length l_{e2} with different width ratios and the length l_{ss} are shown in Fig. 10(a) and (b), respectively. Note that, both the normalized frequencies could be adjusted within a large range by tuning the physical dimensions, which means a flexible bandwidth control operation for the balun implementation. The coupling is enhanced by the proposed CPW-to-slot transitions and an additional transmission pole f_t could be introduced close to the central frequency, which lead to a passband with low insertion loss [20]. In addition, a CPW short-stub [28] is introduced to generate another additional transmission pole f_p and transmission zero f_{zl} for improved in-band performance and lower passband selectivity of the proposed filtering balun, simultaneously. Then, as shown in Fig. 11, a wideband filtering balun with five transmission poles and two transmission zeros is achieved.

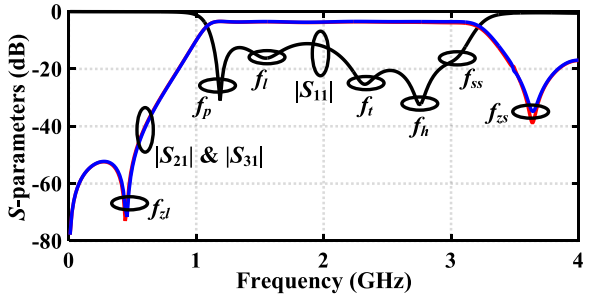

FIGURE 11. Simulated *S*-parameters of the proposed wideband filtering balun (unit: mm. l_{e1} = 3, l_{e2} = 4, l_{n1} = 12.5, l_{n2} = 95, l_{n3} = 13.1, l_o = 3, l_{p1} = 13.2, l_{p2} = 5.94, l_{ss1} = 5.5, l_{ss2} = 4.4, l_{ss3} = 4, s_n = 1.6, s_{ss} = 0.3, w_{e1} = 1, w_{e2} = 7, w_p = 1.76, w_c = 1, w_{ss1} = 3.7, w_{ss2} = 3, and w_{ss3} = 2.3).

B. BALUN WITH FIXED FREQUENCY NOTCH

The balun with fixed frequency notched band (Balun A) is developed based on the balun prototype in Fig. 1(c), as depicted in Fig. 12. Fig. 13(a) shows the simulated notch frequency f_n and calculated electrical length θ_r at notch frequency versus length l_r, while Fig. 13(b) shows the simulated notch frequency f_n and calculated impedance Z_r at notch frequency versus width s_r of the shorted-slot. It is notable that the electrical length θ_r is about $\pi/2$ at the notch frequency. The mismatch between theory and simulation is mainly caused by using the spiral type in slot design for size minimization. Meanwhile, the notch frequency f_n will shift down with length l_r increasing. The impedance Z_r, increasing with width s_r increasing, has a slight impact on the notch frequency in the practical implementation. Then, a wideband filtering balun with a fixed notched band at 2.39 GHz is implemented based on RT5880. The simulated *S*-parameters are shown in Fig. 14.

C. RECONFIGURABLE BALUN WITH TUNABLE DUAL-NOTCHED BANDS

The reconfigurable balun with tunable dual-notched bands (Balun B) is proposed in Fig. 15(a). To change the notched

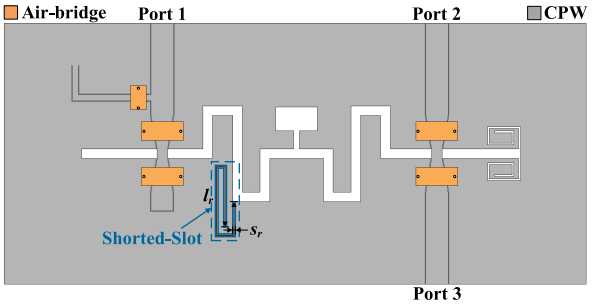

FIGURE 12. Configuration of the proposed balun with fixed frequency notch (Balun A).

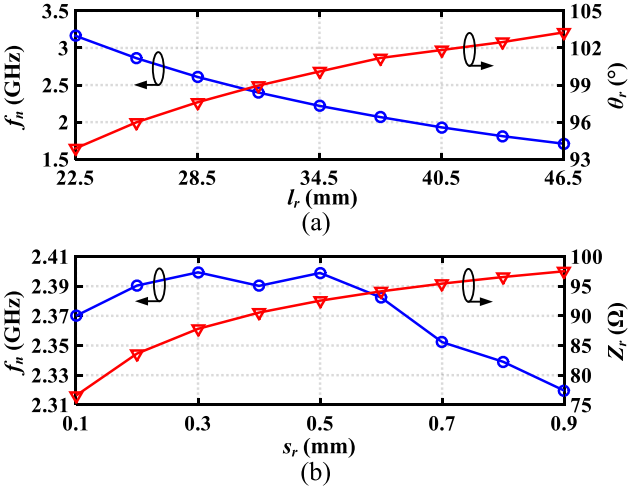

FIGURE 13. (a) Simulated notch frequency f_n and calculated electrical length θ_r at notch frequency versus length l_r (s_r = 0.5 mm). (b) Simulated notch frequency f_n and calculated impedance Z_r at notch frequency versus width s_r of the shorted-slot (l_r = 34.5 mm).

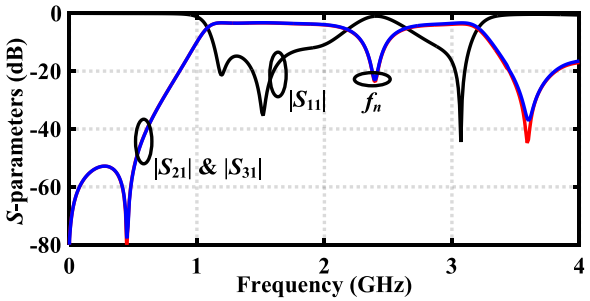

FIGURE 14. Simulated *S*-parameters of the proposed balun with fixed frequency notch ($l_r = 31.5$ mm and $s_r = 0.5$ mm).

band frequency, the length or the gap size of the shorted-slot can be adjusted [29]. In order to accomplish the tunable notched bands, two pairs of varactor-loaded shorted-slots are introduced and they are symmetrical and identical. Besides, diodes are applied for varactors, which can also be used for DC-block capacitances. As shown in Fig. 15(b) and (c), the diode varactors C_a and C_b are connected across the gaps and placed on the bottom layer (i.e., CPW layer). The DC voltage is supplied from the plane with a microstrip line on the top layer and vias are introduced to the both layers. Thus, the DC supply for the diode varactors can be obtained through the vias. RF chokes (10-kΩ resistors) are placed between the DC supply and the diode varactors in order to minimize the RF loss within the frequency range of interest. Moreover, the DC supply and RF chokes are located away from the circuit area of the resonator to eliminate their effects on the shorted-slot.

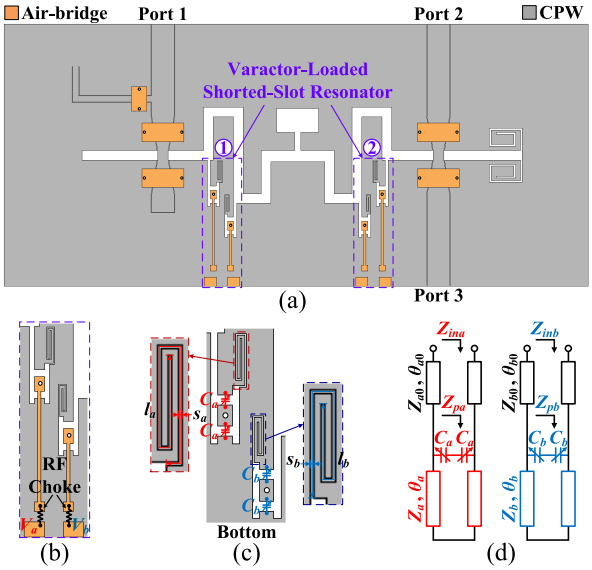

FIGURE 15. The reconfigurable balun with tunable dual-notched bands (Balun B). (a) Configuration. (b) The top view of the varactor-loaded shorted-slot. (c) The bottom layer of the varactor-loaded shorted-slot. (d) The simplified circuit models of the varactor-loaded shorted-slot.

Fig. 15(d) shows the simplified circuit models of the proposed varactor-loaded shorted-slots. Similar to the mechanisms on balun with fixed frequency notch, the transmission

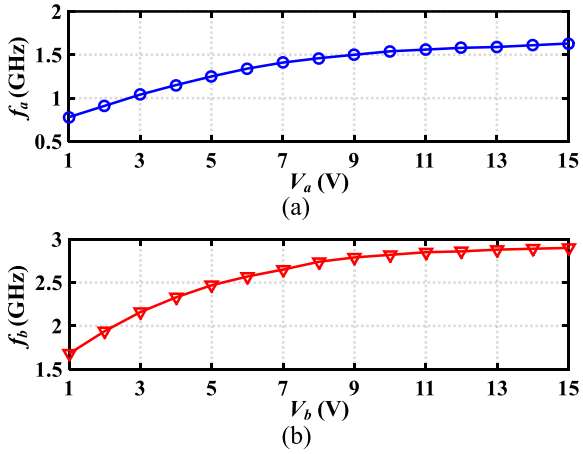

FIGURE 16. The simulated notch frequencies of Balun B ($l_a = 10.8$ mm, $l_b = 9.3$ mm, and $s_a = s_b = 0.1$ mm) with different DC supply (V_a and V_b). (a) The low notch frequency (f_a). (b) The high notch frequency (f_b).

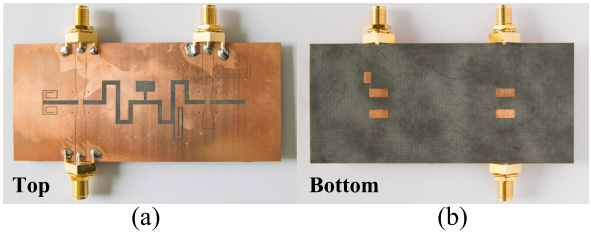

FIGURE 17. Layout of the fabricated balun with fixed frequency notch ($l_r = 31.5$ mm and $s_r = 0.5$ mm). (a) Top view. (b) Bottom view.

zeros (i.e., notches) are generated when input impedances (i.e., Z_{ina} and Z_{inb}) are infinite. Meanwhile, Z_{ina} and Z_{inb} at frequency f could be obtained as

$$Z_{ina,inb} = Z_{a0,b0}\frac{Z_{pa,pb} + jZ_{a0,b0}\tan\theta_{a0,b0}}{Z_{a0,b0} + jZ_{pa,pb}\tan\theta_{a0,b0}} \tag{9}$$

where

$$Z_{pa,pb} = \frac{jZ_{a,b}\tan\theta_{a,b}}{1 - 2\pi f C_{a,b} Z_{a,b}\tan\theta_{a,b}} \tag{10}$$

and Z_a, Z_b, Z_{a0}, Z_{b0}, θ_a, θ_b, θ_{a0}, and θ_{b0} are characteristic impedances and electrical lengths of these two shorted-slots [22], respectively. The Skyworks SMV1232 varactors (C_a) and SMV1235 varactors (C_b) are used in this work. The tuning range for these two capacitances are from 4.15 pF to 0.72 pF and from 18.22 pF to 2.38 pF, respectively, with the applied bias DC voltage varying from 0 V to 15 V. Fig. 16 shows the simulated two notch frequencies of the Balun B when varactors across the gaps have different DC bias. As shown in Fig. 16, the tuning range of the low frequency notch (i.e., f_a) and the high frequency notch (i.e., f_b) are 0.77–1.64 GHz and 1.67–2.91 GHz, which are adjusted by V_a and V_b, respectively. Meanwhile, with the bias DC voltages increasing, the notches will change to high frequency.

TABLE 1. Comparisons with the state-of-the-art filtering baluns.

Ref.	[9]	[12]	[15]	[16]	[17]	[20]	**Balun A**	**Balun B**
f_0 (GHz)	1.07	3.75	6.85	4.0	2.23	2.1	**2.16**	**2.03**
3-dB FBW (%)	112	93	109.5	31.0	56	101.9	**102.6**	**100.5**
A.-Im (dB)	$< \pm 0.4$	$< \pm 0.34$	N/A	$< \pm 0.6$	$< \pm 0.8$	$< \pm 0.31$	$< \pm$**0.503**	$< \pm$**1.1***
P.-Im (°)	$< \pm 2$	$< \pm 3.5$	$< \pm 0.5$	$< \pm 8$	$< \pm 4$	$< \pm 1.3$	$< \pm$**1.54**	$< \pm$**2.6***
IL (dB)	1.07	0.9	0.5	2.0	1	0.458	**0.4**	**1.01**
Group Delay (ns)	N/A	N/A	N/A	N/A	N/A	$<$1.85	$<$**1.89**	$<$**1.94**
Group Delay Variation (ns)	N/A	N/A	N/A	N/A	N/A	$<$1.08	$<$**1.04**	$<$**0.94**
Transmission Zero	Two	Two	None	Two	None	Two	**Two**	**Two**
Notch	0	0	0	0	0	0	**1**	**2**
Fixed/Tunable Notch	–	–	–	–	–	–	**Fixed**	**Tunable**

A.-Im: Amplitude-Imbalance; P.-Im: Phase-Imbalance; $*$: Typical Value

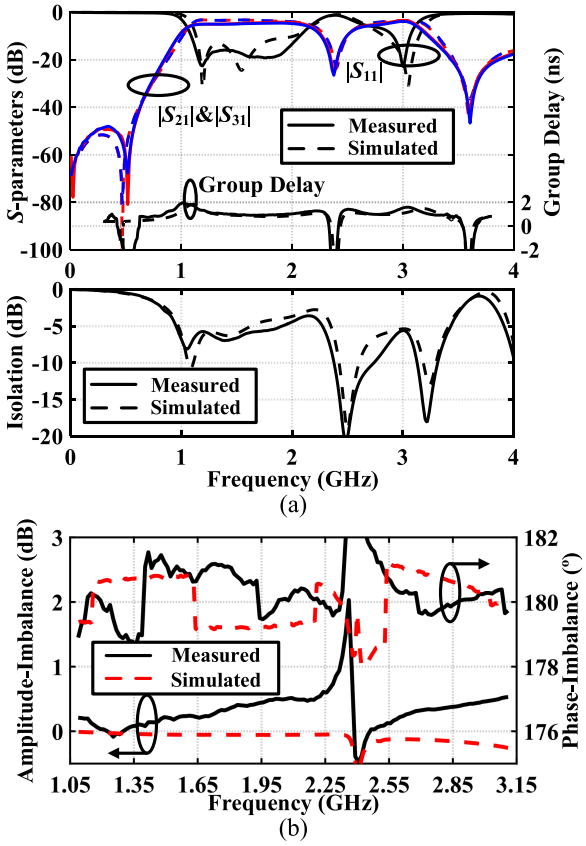

FIGURE 18. Measured and simulated results of the balun with fixed frequency notch. (a) *S*-parameters, isolation, and group delay. (b) Passband magnitude- and phase-imbalances.

III. MEASUREMENTS

To verify the aforementioned mechanisms, a series of baluns (i.e., balun with notched band and reconfigurable balun with dual-notched bands) are implemented on the dielectric substrate RT5880 with $\epsilon_r = 2.2$ and $h = 0.508$ mm. And the *S*-parameter and group delay responses are performed using Keysight 5230A network analyzer.

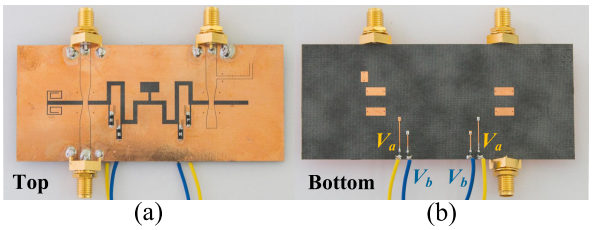

FIGURE 19. Layout of the fabricated balun with tunable dual-notched bands. (a) Top view. (b) Bottom view.

A. BALUN WITH FIXED FREQUENCY NOTCH

A wideband filtering balun with fixed frequency notch is implemented and fabricated. The proposed balun, shown in Fig. 17, exhibits a circuit size including ground of 97.5 mm × 43.6 mm (i.e., $0.76\lambda_g \times 0.34\lambda_g$, where λ_g is the CPW guided-wavelength at the center operation frequency). As shown in Fig. 18(a), the measurement exhibits a wideband passband from 1.05 to 3.26 GHz, which has a narrow notched band at 2.38 GHz with interference suppression level of 24.88 dB. The 10-dB notched FBW of notched bands are 8.8%. The measured minimum insertion loss is found to be 0.4 dB (excluding 3 dB division loss). The simulated and measured amplitude- and phase-imbalances are plotted in Fig. 18(b). It is obvious that the in-band amplitude- and phase-imbalance are less than ±0.503 dB and 180° ± 1.54°, respectively. In addition, it can be observed from Fig. 18 that both the measurement and simulation are in good agreements with each other over a wide band.

B. RECONFIGURABLE BALUN WITH TUNABLE DUAL-NOTCHED BANDS

The reconfigurable balun with tunable dual-notched bands is fabricated with a circuit size including ground of 97.5 mm × 43.6 mm (i.e., $0.76\lambda_g \times 0.34\lambda_g$), as shown in Fig. 19. Fig. 20 depicts the measurements of the reconfigurable balun with tunable dual-notched bands. As it shown, the passband bandwidth is from 1.06 GHz to 3.1 GHz and the minimum in-band insertion loss is 1.01 dB (excluding 3 dB

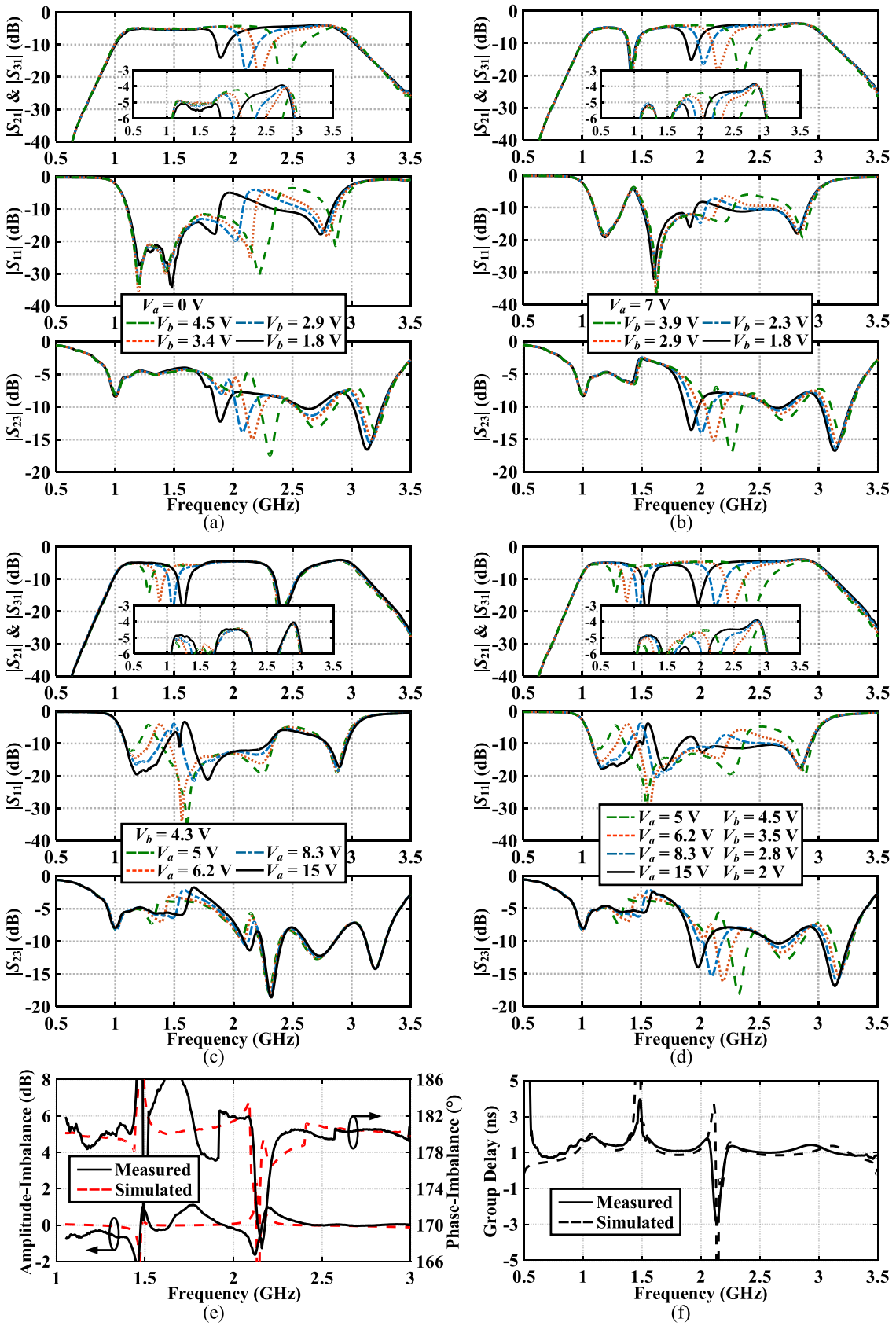

FIGURE 20. (a) Measured case of tuning the high frequency notch with lower notched band switched off. (b) Measured case of tuning the high frequency notch with fixed low frequency notch. (c) Measured case of tuning the low frequency notch with fixed high frequency notch. (d) Measured case of tuning dual-notched bands. Measured and simulated results of (e) passband magnitude- and phase-imbalances and (f) group delay under the case of $V_a = 8.3$ V and $V_b = 2.8$ V.

division loss). Compared to the insertion loss of the wideband filtering balun, the increased insertion loss is mainly caused by the loss of varactor and RF choke resistor. Fig. 20(a) shows the measured S-parameters with the lower notched band switched off. The tuning range of the higher notched band is 24.2% (i.e., 1.89–2.41 GHz) with a rejection level of 15–25.9 dB and a 10-dB notched FBW of 5.2%–9.3%. In Fig. 20(b), as the lower notched band is fixed ($f_1 = 1.41$ GHz), the measured S-parameters are shown. The upper notched band can be tuned from 1.92 GHz to 2.34 GHz with a rejection level of 15.1–22.5 dB. Fig. 20(c) depicts the measured S-parameters while the upper notched band is fixed ($f_2 = 2.4$ GHz). The tuning range for the low-frequency notch is 1.28–1.58 GHz (21.6%) with a rejection level of 15.1–20.3 dB and a 10-dB notched FBW of 3.1%–5.7%. The two notch frequencies can also be tuned, simultaneously, as shown in Fig. 20(d). The simulations and measurements of passband amplitude- and phase-imbalance are shown in Fig. 20(e), under the case of $V_a = 8.3$ V and $V_b = 2.8$ V. It is notable that the in-band amplitude- and phase-imbalances are less than ± 1.1 dB and $180° \pm 2.6°$, respectively. And the group delay under the same case is shown in Fig. 20(f).

A comparison of the proposed wideband filtering baluns with the state-of-the-art researches is shown in Table 1. It indicates that the proposed filtering baluns feature the merits of the wide FBW, low insertion loss, competitive in-band balance, and fixed/tunable notched band operations. To the authors' knowledge, this is the first work on wideband filtering balun with notched bands.

IV. CONCLUSION

In this paper, a wideband filtering balun with tunable dual-notched bands is proposed, implemented, and fabricated. The wideband operation is achieved using the triple-mode slot resonator. The CPW-to-slot transitions are introduced to enhance the amplitude- and phase-imbalance responses. Besides, the CPW short-stub and shorted-slot are employed to improve the passband selectivity. Two pairs of the varactor-loaded shorted-slots are introduced to achieve the tunable notched band operation. The proposed reconfigurable balun exhibits the high merits of the wide fractional bandwidth, low insertion loss, good in-band balance performance, and tunable notched band operation, simultaneously. Good agreements between the measured and simulated results are achieved. With such good performance, the balun prototypes are attractive for practical applications in wideband cognitive radios with high interference levels.

APPENDIX

A. CHARACTERISTIC IMPEDANCE AND ELECTRICAL LENGTH OF SLOT

As depicted in [22], the characteristic impedance Z_0 and guided-wavelength λ of a slot within $0.0015 \le s/\lambda_0 \le 0.075$ can be expressed as

$$\begin{aligned} Z_0 = {} & 60 + 3.69 \sin\left[\frac{(\epsilon_r - 2.22)\pi}{2.36}\right] + 133.5 \ln(10\epsilon_r)\sqrt{\frac{s}{\lambda_0}} \\ & + 2.81[1 - 0.011\epsilon_r(4.48 + \ln\epsilon_r)]\left(\frac{s}{h}\right)\ln\left(\frac{100h}{\lambda_0}\right) \\ & + 131.1(1.028 - \ln\epsilon_r)\sqrt{\frac{h}{\lambda_0}} \\ & + 12.48\frac{(1 + 0.18\ln\epsilon_r)s}{h\sqrt{\epsilon_r - 2.06 + 0.85(\frac{s}{h})^2}} \end{aligned} \tag{11}$$

and

$$\lambda = \lambda_0\left[A - B\ln\left(\frac{h}{\lambda_0}\right)\right] \tag{12}$$

where

$$A = 1.045 - 0.365\ln\epsilon_r + \frac{6.3\left(\frac{s}{h}\right)\epsilon_r^{0.945}}{238.64 + 100\left(\frac{s}{h}\right)} \tag{13}$$

$$B = 0.148 - \frac{8.81(\epsilon_r + 0.95)}{100\epsilon_r} \tag{14}$$

where ϵ_r is the dielectric constant, h is the thickness of substrate, and s is the width of the slot. λ_0 is the free space wavelength (i.e., $\lambda_0 = c/f$, where c is the velocity of light in free space and f is the operation frequency). Then, the electrical wavelength θ of a slot with physical length l can be calculated as

$$\theta = 2\pi \times \frac{l}{\lambda} = \frac{2\pi l}{\lambda_0\left[A - B\ln\left(\frac{h}{\lambda_0}\right)\right]}. \tag{15}$$

B. EQUIVALENT RLC RESONATOR MODEL OF AIR-BRIDGE

The simplified series resonator model of the air-bridge is shown in Fig. 3(b). As depicted in [24], the relationship between the transmission coefficient and R_s, L_s, and C_s may be expressed as

$$|S_{21}|^2 = \frac{4\left(1 - \omega^2 L_s C_s\right)^2 + 4R_s^2\omega^2}{4\left(1 - \omega^2 L_s C_s\right)^2 + \omega^2 C_s^2\left(2R_s + Z_0\right)^2}. \tag{16}$$

From (21), R_s can be obtained from $|S_{21}|$, at the first resonant frequency as

$$R_s = \left.\frac{Z_0|S_{21}|}{2\left(1 - |S_{21}|\right)}\right|_{\omega_{res}} \tag{17}$$

and L_s can also be calculated by choosing the bandwidth $(\omega_2 - \omega_1)$ with $S_{21} = a$, at $\omega = \omega_1, \omega_2$,

$$L_s = \frac{\sqrt{a^2\left(2R_s + Z_0\right)^2 - 4R_s^2}}{2\left(\omega_2 - \omega_1\right)\sqrt{1 - a^2}}. \tag{18}$$

Then, C_s will be obtained by substituting L_s into the equation as follow,

$$C_s = \frac{1}{\omega_{res}^2 L_s}. \tag{19}$$

REFERENCES

[1] L. K. Yeung and K.-L. Wu, "An LTCC balanced-to-unbalanced extracted-pole bandpass filter with complex load," *IEEE Trans. Microw. Theory Techn.*, vol. 54, no. 4, pp. 1512–1518, Jun. 2006.
[2] H. H. Ta, B. Pham, A.-V. Pham, and R. E. Leoni, "A 23:1 bandwidth ratio balun on multilayer organic substrate," in *IEEE MTT-S Int. Microw. Symp. Dig.*, Seattle, WA, USA, Jun. 2013, pp. 1–3.
[3] Y. Peng, T. Wang, Y. M. Huang, W. Jiang, and G. Wang, "Electrically tunable bandpass filtering balun on engineered substrate embedded with patterned Permalloy thin film," in *IEEE MTT-S Int. Microw. Symp. Dig.*, San Francisco, CA, USA, May 2016, pp. 1–3.
[4] T. Yang, M. Tamura, and T. Itoh, "Compact hybrid resonator with series and shunt resonances used in miniaturized filters and balun filters," *IEEE Trans. Microw. Theory Techn.*, vol. 58, no. 2, pp. 390–402, Feb. 2010.
[5] C.-H. Wu, C.-H. Wang, S.-Y. Chen, and C. H. Chen, "Balanced-to-unbalanced bandpass filters and the antenna application," *IEEE Trans. Microw. Theory Techn.*, vol. 56, no. 11, pp. 2474–2482, Nov. 2008.
[6] G. S. Huang and C. H. Chen, "Dual-band balun bandpass filter with hybrid structure," *IEEE Microw. Wireless Compon. Lett.*, vol. 21, no. 7, pp. 356–358, Jul. 2011.
[7] P. Cheong, T.-S. Lv, W.-W. Choi, and K.-W. Tam, "A compact microstrip square-loop dual-mode balun-bandpass filter with simultaneous spurious response suppression and differential performance improvement," *IEEE Microw. Wireless Compon. Lett.*, vol. 21, no. 2, pp. 77–79, Feb. 2011.
[8] W. Feng and W. Che, "Wideband balun bandpass filter based on a differential circuit," in *IEEE MTT-S Int. Microw. Symp. Dig.*, Montreal, QC, Canada, Jun. 2012, pp. 1–3.
[9] Y.-W. Lin, J.-C. Lu, and C.-Y. Chang, "Design of high-order wideband planar balun filter in *S*-plane bandpass prototype," *IEEE Trans. Microw. Theory Techn.*, vol. 60, no. 7, pp. 2124–2130, Jul. 2012.
[10] S. Lin, J. Wang, G. Zhang, and J.-S. Hong, "Design of microstrip tri-mode balun bandpass filter with high selectivity," *Electron. Lett.*, vol. 51, no. 13, pp. 998–999, Jun. 2015.
[11] J. H. Lee, J. A. Park, C. S. Cho, and J. W. Lee, "New design formulas for asymmetric coupled-section Marchand balun," *IEEE Microw. Wireless Compon. Lett.*, vol. 25, no. 7, pp. 448–450, Jul. 2015.
[12] F. Huang, J. Wang, J. Hong, and W. Wu, "Wideband balun bandpass filter with broadside-coupled microstrip/slotline resonator structure," *Electron. Lett.*, vol. 53, no. 19, pp. 1320–1321, Sep. 2017.
[13] X. Guo, L. Zhu, J. Wang, and W. Wu, "Wideband microstrip-to-microstrip vertical transitions via multiresonant modes in a slotline resonator," *IEEE Trans. Microw. Theory Techn.*, vol. 63, no. 6, pp. 1902–1909, Jun. 2015.
[14] A. M. H. Nasr and A. M. E. Safwat, "Multimode coplanar waveguide cross-junction: Equivalent circuit model and air-bridge free applications," *IEEE Trans. Microw. Theory Techn.*, vol. 65, no. 10, pp. 3753–3760, Oct. 2017.
[15] M. E. Bialkowski and A. M. Abbosh, "Design of a compact UWB out-of-phase power divider," *IEEE Microw. Wireless Compon. Lett.*, vol. 17, no. 4, pp. 289–291, Apr. 2007.
[16] D. Chen, L. Zhu, H. Bu, and C. Cheng, "A wideband balun filter on a triple-mode slotline resonator with controllable bandwidth," *IEEE Microw. Wireless Compon. Lett.*, vol. 27, no. 6, pp. 569–571, Jun. 2017.
[17] A. A. Ibrahim, A. M. E. Safwat, and H. El-Hennawy, "Uniplanar bridgeless CPW-to-slotline transition and its application to CPW balun," *Electron. Lett.*, vol. 48, no. 8, pp. 443–444, Apr. 2012.
[18] H. Wang, K.-W. Tam, S.-K. Ho, W. Kang, and W. Wu, "Design of ultra-wideband bandpass filters with fixed and reconfigurable notch bands using terminated cross-shaped resonators," *IEEE Trans. Microw. Theory Techn.*, vol. 62, no. 2, pp. 252–265, Feb. 2014.
[19] D. Psychogiou, R. Gómez-García, and D. Peroulis, "Wide-passband filters with in-band tunable notches for agile multi-interference suppression in broad-band antenna systems," in *Proc. IEEE Radio Wireless Symp.*, Anaheim, CA, USA, Jan. 2018, pp. 213–216.
[20] J. Ren, H. J. Qian, J. Zhou, and X. Luo, "A wideband filtering balun using CPW-to-slotline transitions," in *IEEE MTT-S Int. Microw. Symp. Dig.*, Jun. 2018, pp. 1–3.
[21] J. P. Kim and W. S. Park, "An improved network modeling of slot-coupled microstrip lines," *IEEE Trans. Microw. Theory Techn.*, vol. 46, no. 10, pp. 1484–1491, Oct. 1998.
[22] R. Janaswamy and D. H. Schaubert, "Characteristic impedance of a wide slotline on low-permittivity substrates (short paper)," *IEEE Trans. Microw. Theory Techn.*, vol. MTT-34, no. 8, pp. 900–902, Aug. 1986.
[23] S.-C. Lin, T.-N. Kuo, Y.-S. Lin, and C. H. Chen, "Novel coplanar-waveguide bandpass filters using loaded air-bridge enhanced capacitors and broadside-coupled transition structures for wideband spurious suppression," *IEEE Trans. Microw. Theory Techn.*, vol. 54, no. 8, pp. 3359–3369, Aug. 2006.
[24] C.-C. Chang, C. Caloz, and T. Itoh, "Analysis of a compact slot resonator in the ground plane for microstrip structures," in *Proc. Asia–Pacific Microw. Conf.*, Dec. 2001, pp. 1100–1103.
[25] G. Duchamp, L. Casadebaig, S. Gauffre, and J. Pistre, "An alternative method for end-effect characterization in shorted slotlines," *IEEE Trans. Microw. Theory Techn.*, vol. 46, no. 11, pp. 1793–1795, Nov. 1998.
[26] J.-S. Hong and M. J. Lancaster, *Microstrip Filters for RF/Microwave Applications*. New York, NY, USA: Wiley, 2001.
[27] Z.-A. Ouyang and Q.-X. Chu, "Novel septuple-mode balanced filter with enhanced selectivity and extended upper-stopband using multi-mode slotline structure," in *IEEE MTT-S Int. Microw. Symp. Dig.*, San Francisco, CA, USA, May 2016, pp. 1–3.
[28] F. Aryanfar and K. Sarabandi, "Characterization of semilumped CPW elements for Millimeter-wave filter design," *IEEE Trans. Microw. Theory Techn.*, vol. 53, no. 4, pp. 1288–1293, Apr. 2005.
[29] S. A. Aghdam, "Reconfigurable antenna with a diversity filtering band feature utilizing active devices for communication systems," *IEEE Trans. Antennas Propag.*, vol. 61, no. 10, pp. 5223–5228, Oct. 2013.

JIE ZHOU (S'16) received the B.E. degree in microelectronics from the University of Electronic Science and Technology of China, Chengdu, China, in 2016, where he is currently pursuing the Ph.D. degree in microelectronics and solid-state electronics.

His current research interests include the RF/microwave/millimeter-wave transmitter and reconfigurable phase shifter, especially integrated circuits.

Mr. Zhou was a recipient of the IEEE MTT-Society Undergraduate/Pre-Graduate Scholarship Award, in 2017.

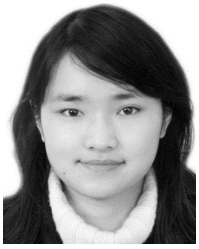

HUIZHEN JENNY QIAN received the B.E., master's, and Ph.D. degrees in electronic engineering from the University of Electronic Science and Technology of China (UESTC), Chengdu, China, in 2008, 2011, and 2018, respectively.

She is currently an Assistant Professor with the Center for Integrated Circuits, UESTC. Her research interests include the wideband microwave/millimeter-wave transceiver, reconfigurable passive circuits, and on-chip array systems.

Dr. Qian was a recipient of the 2018 IEEE MTT-Society Graduate Fellowship Award, the IEEE IWS Best Student Paper Award, in 2018 (Second Place) and 2015 (First Place), the IEEE IMS Student Design Competition Award, in 2018 (Second Place) and 2017 (First Place), and the IEEE RFIT Best Student Paper Award, in 2016.

JIYUAN REN received the B.E. degree in electronic science and technology from Sichuan University, Chengdu, China, in 2017. He is currently pursuing the master's degree in integrated circuit engineering with the University of Electronic Science and Technology of China.

His current research interests include the wideband filters and passive components.

XUN LUO (S'08–M'11–SM'12) received the B.E. and Ph.D. degrees in electronic engineering from the University of Electronic Science and Technology of China (UESTC), Chengdu, China, in 2005 and 2011, respectively.

From 2010 to 2013, he was with Huawei Technologies Co., Ltd., as the Project Manager to guide R&D projects of multi-band microwave/millimeter-wave integrated systems for backhaul and wireless communication. Since 2015, he has been with UESTC as a Full Professor and has been appointed as the Executive Director of the Center for Integrated Circuits. Before joining UESTC, he was an Assistant Professor with the Department of Microelectronics, Delft University of Technology. He has authored or co-authored about 70 journal and conference papers. He holds/filed more than 50 patents. His research interests include the RF/microwave/mm-wave integrated circuits, multiple-resonance THz modules, multi-bands backhaul/wireless systems, reconfigurable passive circuits, smart antennas, and system in package.